Title

Functional Modeling Identifies Paralogous Solanesyl-diphosphate Synthases That Assemble the Side Chain of Plastoquinone-9 in Plastids*

Journal

Journal of Biological Chemistry, 288(38)

ISSN

0021-9258

Authors

Block, Anna
Fristedt, Rikard
Rogers, Sara
et al.

Publication Date

2013-09-01

DOI

10.1074/jbc.m113.492769

THE JOURNAL OF BIOLOGICAL CHEMISTRY VOL. 288, NO. 38, pp. 27594–27606, September 20, 2013

Functional Modeling Identifies Paralogous Solanesyl-diphosphate Synthases That Assemble the Side Chain of Plastoquinone-9 in Plastids*[S]

Received for publication, June 11, 2013, and in revised form, August 2, 2013 Published, JBC Papers in Press, August 2, 2013, DOI 10.1074/jbc.M113.492769

Anna Block[‡1], **Rikard Fristedt**[§1], **Sara Rogers**[‡], **Jyothi Kumar**[‡], **Brian Barnes**[‡], **Joshua Barnes**[‡], **Christian G. Elowsky**[‡], **Yashitola Wamboldt**[‡], **Sally A. Mackenzie**[‡], **Kevin Redding**[¶], **Sabeeha S. Merchant**[§], **and Gilles J. Basset**[‡2]

From the [‡]*Center for Plant Science Innovation, University of Nebraska, Lincoln, Nebraska 68588, the* [§]*Department of Chemistry and Biochemistry, University of California, Los Angeles, California 90095, and the* [¶]*Department of Chemistry and Biochemistry, Arizona State University, Tempe, Arizona 85287*

Background: Plastid isoforms of solanesyl-diphosphate synthase catalyze the elongation of the prenyl side chain of plastoquinone-9.
Results: Corresponding mutants display lower levels of plastoquinone-9 and plastochromanol-8 and display intact levels of vitamin E.
Conclusion: Plastochromanol-8 originates from a subfraction of non-photoactive plastoquinol-9 and is not essential for seed longevity.
Significance: Viable plastoquinone-9 mutants are invaluable tools for understanding plastid metabolism.

It is a little known fact that plastoquinone-9, a vital redox cofactor of photosynthesis, doubles as a precursor for the biosynthesis of a vitamin E analog called plastochromanol-8, the physiological significance of which has remained elusive. Gene network reconstruction, GFP fusion experiments, and targeted metabolite profiling of insertion mutants indicated that *Arabidopsis* possesses two paralogous solanesyl-diphosphate synthases, AtSPS1 (*At1g78510*) and AtSPS2 (*At1g17050*), that assemble the side chain of plastoquinone-9 in plastids. Similar paralogous pairs were detected throughout terrestrial plant lineages but were not distinguished in the literature and genomic databases from mitochondrial homologs involved in the biosynthesis of ubiquinone. The leaves of the *atsps2* knock-out were devoid of plastochromanol-8 and displayed severe losses of both non-photoactive and photoactive plastoquinone-9, resulting in near complete photoinhibition at high light intensity. Such a photoinhibition was paralleled by significant damage to photosystem II but not to photosystem I. In contrast, in the *atsps1* knock-out, a small loss of plastoquinone-9, restricted to the non-photoactive pool, was sufficient to eliminate half of the plastochromanol-8 content of the leaves. Taken together, these results demonstrate that plastochromanol-8 originates from a subfraction of the non-photoactive pool of plastoquinone-9. In contrast to other plastochromanol-8 biosynthetic mutants, neither the single *atsps* knock-outs nor the *atsps1 atsps2* double knock-out displayed any defects in tocopherols accumulation or germination.

Plastoquinone-9 (2,3-dimethyl-6-solanesyl-1,4-benzoquinone) is a vital redox cofactor for oxygenic photoautotrophs. It is required during photosynthesis for electron transfer and proton translocation in thylakoid membranes, as well as for respiration in cyanobacteria and as a necessary oxidant for the desaturation of the carotenoid precursor phytoene (1–3). Furthermore, it is via the redox state of plastoquinone-9 in thylakoid membranes that plants and cyanobacteria monitor the balance of photosystem II and photosystem I activity and adjust the expression of some plastid and nuclear genes (4, 5).

Plastoquinone-9 is a bipartite molecule made up of a redox active benzoquinone ring attached to a solanesyl (C_{45}) chain (Fig. 1). Plants derive the benzenoid moiety from homogentisate, which is prenylated and decarboxylated in the inner envelope of chloroplasts, yielding 2-methyl-6-solanesyl-1,4-benzoquinol (6, 7). The latter is then methylated to give plastoquinol-9 (Fig. 1). Analogy with the assembly of the polyprenyl side chain of ubiquinone in proteobacteria and mitochondria indicates that the biosynthesis of the plastoquinone-9 solanesyl moiety proceeds from the *trans*-long chain prenyl-diphosphate synthase-catalyzed elongation of a C_{15}–C_{20} allylic diphosphate precursor. The corresponding activity has therefore been tentatively attributed in *Arabidopsis* and rice to plastid-targeted solanesyl-diphosphate synthases, products of the *At1g17050* and *Os05g0582300* genes, respectively (8–10), although there is no direct evidence that such enzymes indeed participate in plastoquinone-9 biosynthesis. A peculiarity of the biosynthetic pathway of plastoquinone-9 in photosynthetic eukaryotes is

* This work was made possible in part by National Science Foundation Grants MCB-0918258 and MCB-1148968 (to G. J. B.), United States Department of Energy Cooperative Agreements DE-FC02-02ER63421 (to S. S. M.) and DE-FG02-12ER16189 (to S. A. M.), and a Wenner-Gren Foundation grant (to R. F.). This work was also supported by the Center for Plant Science Innovation and the Department of Biochemistry at the University of Nebraska-Lincoln.

Sequence data from this article can be found in the GenBank™/EBI Data Bank, and a list of their accession numbers is provided in supplemental Data File 1.

[S] This article contains supplemental Data File 1.

[1] Both authors contributed equally to this work.

[2] To whom correspondence should be addressed: Ctr. for Plant Science Innovation, Beadle Ctr. for Genetic Research, University of Nebraska, Lincoln, NE 68588. Tel.: 402-472-2930; Fax: 402-472-3139; E-mail: gbasset2@unl.edu.

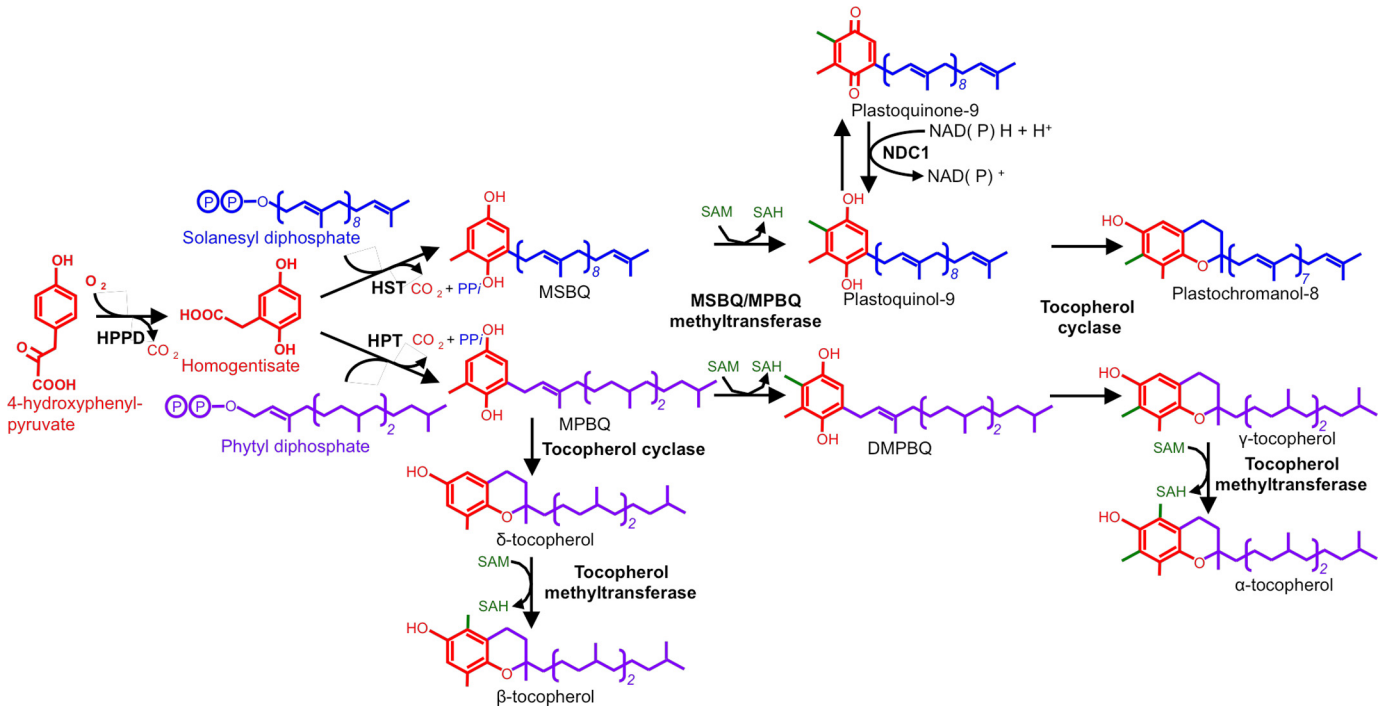

FIGURE 1. **Metabolic connections among the biosynthetic pathways of plastoquinone-9, plastochromanol-8, and tocopherols in plants.** Knock-out mutants corresponding to HPPD, HST, and MSBQ/MPBQ methyltransferase are devoid of plastoquinone-9 and are seedling-lethal. *DMPBQ*, 2,3-dimethyl-5-phytyl-1,4-benzoquinone; *HPPD*, 4-hydroxyphenylpyruvate dioxygenase; *HPT*, homogentisate phytyl transferase; *HST*, homogentisate solanesyl transferase; *MPBQ*, 2-methyl-6-phytyl-1,4-benzoquinol; *MSBQ*, 2-methyl-6-solanesyl-1,4-benzoquinol; *NDC1*, NAD(P)H quinone oxidoreductase C1; *SAH*, *s*-adenosyl-homocysteine; *SAM*, *s*-adenosyl-methionine.

that it intertwines with that of tocopherols (Fig. 1). First, the hydroxychroman moiety of tocopherols also originates in part from homogentisate (6). Second, the methyltransferase that decorates the benzoquinol ring intermediate also functions in the biosynthesis of tocopherols (11). Lastly, plastoquinol-9 itself can serve as a substrate for tocopherol cyclase to yield plastochromanol-8 in plastoglobules (12, 13). Although it has received considerably less attention than tocopherols, plastochromanol-8 is thought to function as an antioxidant in plants. This seems a valid possibility, because plastochromanol-8 contains the same hydroxychroman ring as γ-tocopherol (Fig. 1), and hydroxyplastochromanol-8, formed as a result of singlet oxygen scavenging by plastochromanol-8, has been shown to accumulate in leaves during high light stress and aging (14). In particular, there is evidence that the seeds of an *Arabidopsis* mutant unable to synthesize either plastochromanol-8 or tocopherols exhibit increased lipid oxidation during desiccation and quiescence, resulting in lower seed longevity compared with those of another mutant that is devoid of tocopherols only (15). However, it is unclear to what extent plastochromanol-8 contributes to the antioxidant arsenal of plant tissues when tocopherols are present, as would normally happen in nature. In fact, studying the specific roles of plastoquinone-9 and plastochromanol-8 by means of straightforward loss-of-function strategies has invariably proved vexing. Not only is the biosynthesis of plastoquinone-9 and plastochromanol-8 seemingly impossible to disconnect from that of tocopherols, but all of the plastoquinone-9 biosynthetic mutants identified to date, namely those corresponding to 4-hydroxyphenylpyruvate dioxygenase, homogentisate solanesyl transferase, and 2-methyl-6-solanesyl-1,4-benzoquinol methyltransferase (Fig. 1), are albino and seedling-lethal (3, 11, 16).

In this study, we demonstrated that *Arabidopsis thaliana* possesses two solanesyl-diphosphate synthases involved in the assembly of the plastoquinone-9 side chain. We then examined the impact of a deficit of plastoquinone-9, plastoquinol-9, and plastochromanol-8 in the leaves and seeds of cognate mutants, the tocopherol biosynthetic capabilities of which are intact.

MATERIALS AND METHODS

Chemicals and Reagents—Ubiquinone-10 was from Sigma-Aldrich. α-Tocopherol was from Acros Organics, and δ-tocopherol and γ-tocopherol were from Matreya, LLC. Ubiquinone-9, plastoquinone-9, and plastochromanol-8 standards were extracted from *Candida utilis*, *Synechocystis* sp. PCC 6803, and the seeds of *Camelina sativa*, respectively, and HPLC-purified. Quinol standards were synthesized chemically from the reduction of their corresponding quinone forms using sodium borohydride. Calibration solutions were quantified spectrophotometrically using the molar extinction coefficients of 14,600 $M^{-1}\cdot cm^{-1}$ at 275 nm for ubiquinone, 15,200 $M^{-1}\cdot cm^{-1}$ at 255 nm for plastoquinone-9, 3260 $M^{-1}\cdot cm^{-1}$ at 292 nm for α-tocopherol, 3510 $M^{-1}\cdot cm^{-1}$ at 298 nm for δ-tocopherol, and 3810 $M^{-1}\cdot cm^{-1}$ at 298 nm for γ-tocopherol (17) and the absorbance value $E_{1\ cm}$ (1%) at 296 nm = 55.5 for plastochromanol-8 (18). High fidelity PCR amplifications were performed with Phusion polymerase (Finnzymes), and PCR genotyping experiments were performed with GoTaq polymerase

(Promega). All DNA constructs were verified by sequencing. Unless mentioned otherwise, all other reagents were from Fisher Scientific.

Plant Material and Growth Conditions—*Arabidopsis* T-DNA insertion mutant SALK_126948 (*At1g78510; AtSPS1*) and SALK_064292 (*At1g17050; AtSPS2*) were obtained from the Arabidopsis Biological Resource Center at the Ohio State University (19). Seeds were allowed to germinate *in vitro* on Murashige and Skoog solid medium and transferred to potting mix in a growth chamber at 22 °C in 16-h days (110 $\mu E \cdot m^{-2} \cdot s^{-1}$) for 4 weeks. The double knock-out was obtained from the F2 segregating progeny resulting from the cross between the individual SALK_126948 and SALK_064292 homozygous T-DNA mutants. For the measurements of chlorophyll fluorescence and metabolite quantification during acclimation to high light, plants were grown directly on soil under moderate light intensity (110–120 $\mu E \cdot m^{-2} \cdot s^{-1}$) for 3 weeks and then switched to high light intensity (600–800 $\mu E \cdot m^{-2} \cdot s^{-1}$). For germination assays, *Arabidopsis* seeds stored previously at 4 °C with silica gel as a desiccant were subjected to accelerated aging for 72 h at 40 °C and 100% of relative hygrometry and then vernalized for 5 additional days at 4 °C to break dormancy as described previously (20). Unaged controls were vernalized directly. Seeds were then surface-sterilized with sodium hypochlorite and plated on Murashige and Skoog medium containing sucrose (10 g/liter). Plates were placed in 16-h days (110 $\mu E \cdot m^{-2} \cdot s^{-1}$) at 22 °C, and germination was scored after 3 weeks by the emergence of the radical root.

Plant Genotyping and RT-PCR Analyses—*Arabidopsis* plants were genotyped using a combination of primers: LP1, 5′-TCGTGTATCAAGCTTGCAGTG-3′; RP1, 5′-ATGATCTCATGTGGGCTTGTC-3′; T-DNA-specific LBb1, 5′-GCGTGGACCGCTTGCTGCAACT-3′ (*SPS1*, SALK_126948); LP2, 5′-TTACATCTTTGACCGCGAAAC-3′; RP2, 5′-AATCAAAGAAGATAAACAATAATTAT-3′; and T-DNA-specific LBb1 (*SPS2*, SALK_064292). To determine the exact location of the T-DNA insertion in SALK_064292 mutant, a 1167-bp genomic fragment was amplified using the primer pair LP2+LBb1, cloned in pGEM-T Easy (Promega), and sequenced from the T7 and SP6 priming sites of the vector. For RT-PCR analysis, total RNA from *Arabidopsis* leaves was extracted using the SV total RNA isolation system (Promega). PCR was performed on cDNAs prepared from 500 ng of total RNA using the following gene-specific primers: RTfwd1, 5′-AAACAGCCTATTTCGTTGGTG-3′), and RTrvs1, 5′-TCACATCAGGCTCAACTCTG-3′ for *AtSPS1*; RTfwd2, 5′-GGTATTTCTCCGGCGAGATT-3′, and RTrvs2, 5′-GCGACCTTGCTTTCGACTTTA-3′, for *AtSPS2*; and 5′-CTAAGCTCTCAAGATCAAAGGC-3′ (forward) and 5′-TTAACATTGCAAAGAGTTTCAAGG-3′ (reverse) for the actin control.

Subcellular Localization—For expression of the AtSPS1-GFP fusion under the control of the *AtSPS1* native promoter, a 3089-bp genomic DNA fragment comprising the *At1g78510* sequence (minus its stop codon) up to the second exon of the 5′ upstream gene (*At1g78520*) was amplified using primers 5′-AACGAAACTTCATCAACGTC-3′ (forward) and 5′-AAGATT*ACTAGT*ATCAATTCTTTCGAGGTTATACAA-3′ (reverse), with the latter containing an SpeI restriction site (italicized). The amplified product was cut with SpeI and ligated into EcoRI (blunted)/SpeI-digested pCAMBIA-1302C (21), replacing the 35S promoter of the vector and resulting in an in-frame fusion with the N-terminal end of GFP. This construct was electroporated into *Agrobacterium tumefaciens* C58C1, and the transformed cells were infiltrated into the leaves of *Nicotiana benthamiana*. Tobacco epidermal cells were imaged by confocal laser scanning microscopy 48 h later. For imaging in *Arabidopsis* plants, the pCAMBIA-*AtSPS1-GFP* construct was stably introduced using the floral dip method (22).

Terpenoid Conjugates Analyses—*Arabidopsis* leaf (36–94 mg of fresh weight) and seed (35–45 mg) samples were spiked with 6.2–6.9 nmol of ubiquinone-10 and homogenized in 0.5 ml of 95% (v/v) ethanol using a 5-ml Pyrex tissue grinder. For the quantification of plastoquinol-9 in illuminated leaves (determination of photoactive pool), care was taken to maintain exposure to high light intensity until tissues were completely disrupted. Trial experiments showed that there was no post-mortem photoreduction of plastoquinone-9. The grinder was rinsed with 0.2 ml of 95% (v/v) ethanol, and the wash was combined with the original extract. The sample was then centrifuged (5 min at 18,000 × *g*) and immediately analyzed by HPLC on a 5 μM Supelco Discovery C-18 column (250 × 4.6 mm, Sigma-Aldrich) thermostatted at 30 °C and developed in isocratic mode at a flow rate of 1.5 ml min^{-1} with methanol. Plastoquinone-9 and ubiquinone-10 were detected spectrophotometrically at 255 and 275 nm, respectively. Plastoquinol-9, plastochromanol-8, and tocopherols were detected fluorometrically (290 and 330 nm for excitation and emission, respectively). Retention times were 5.3 min (δ-tocopherol), 5.9 min (γ-tocopherol), 6.6 min (α-tocopherol), 14.3 min (plastoquinol-9), 28.4 min (plastochromanol-8), 40.7 min (plastoquinone-9), and 45.1 min (ubiquinone-10). Compounds were quantified according to their corresponding external calibration standards, and data were corrected for recovery of the ubiquinone-10 internal standard. Ubiquinone-9 was quantified as described previously (23).

Analysis of Photosystems—Imaging of maximum quantum efficiency of photosystem II on whole *Arabidopsis* plants was performed using a FluorCam 700 MF system (Photon Systems Instruments) using the quenching analysis effect settings. Pulses of actinic light and continuous illumination were generated by two arrays, each made up of 345 620 nm-LEDs. Plants were dark-adapted for 20 min before each experiment. Fluorescence parameters were calculated as follows: $F_v/F_m = (F_m - F_o)/F_m$, where F_v is the calculated variable fluorescence, F_m is the maximal fluorescence measured immediately after the saturating pulse, and F_o is the initial fluorescence of dark-adapted tissues; $R_{fd} = F_d/F_s$, where F_d is the fluorescence decrease from F_m to F_s (the steady state fluorescence measured after 3 s of continuous illumination); non-photochemical quenching (NPQ) = $(F_m - F_m')/F_m'$, where F_m' is the maximal fluorescence measured after a 3-s adaptation to actinic light; photoinhibition = $1 - (F_v''/F_m'')/(F_v/F_m)$, where F_v'' and F_m'' are the variable and maximal fluorescence, respectively, measured after 2, 24, and 48 h of exposure to actinic light at 800 $\mu E \cdot m^{-2} \cdot s^{-1}$ followed by 20 min of recovery in the dark. The

kinetics of photosystem I photoxidation were measured on detached leaves using a JTS-10 LED spectrometer (Bio-Logic Scientific Instruments) in absorbance detection mode. P700 was oxidized using 10-ms actinic flashes of far-red LEDs and a 705-nm interference filter. Base-line absorbances were obtained without actinic illumination and subtracted. Chloroplast preparation and separation of proteins by SDS-PAGE for the immunodetection of subunits D1 and PsaA were performed as described previously (24). Anti-D1 and anti-PsaA antibodies were from Agrisera and Dr. J. D. Rochaix's laboratory (University of Geneva), respectively. Immunoreactive proteins were visualized using the SuperSignal West Pico HRP detection kit (Thermo Scientific) according to the manufacturer recommendations.

RESULTS

Modeling of Gene Co-expression Network Predicts That Arabidopsis Possesses Two Solanesyl-Diphosphate Synthases That Functionally Intersect in Plastids—BLASTp searches of *Arabidopsis* genomic databases using either *Escherichia coli* octaprenyl-diphosphate synthase (IspB) or *Saccharomyces cerevisiae* hexaprenyl-diphosphate synthase (Coq1) as queries, both of which assemble the side chain of ubiquinone in their respective hosts (25, 26), detected three proteins that bear the molecular attributes of *trans*-long chain diphosphate synthases, At1g78510, At1g17050, and At2g34630. As previous reports indicate that all three of these proteins harbor solanesyl-diphosphate synthase activity (9, 27, 28), we shall call them hereafter, for purpose of clarity, AtSPS1, AtSPS2, and AtSPS3, respectively. Modeling of a high stringency network made up of the top 100 genes (0.45% of the 22,263 expressed loci in the ATTED-II database) that co-express with AtSPS1, AtSPS2, and AtSPS3 generated six gene clusters (Fig. 2). Three of those clusters corresponded to genes that uniquely co-express with *AtSPS1*, *AtSPS2*, or *AtSPS3*, two to genes that co-express either with *AtSPS1* and *AtSPS2* or with *AtSPS1* and *AtSPS3*, and one to genes that co-express with all three *AtSPS* members (Fig. 2). (Supplemental Data File 1 provides a list of these genes including their correlation rank and functional annotations.) Subcellular localization data compiled from the SUBA and TAIR databases were then overlaid on each cluster (Fig. 2). Remarkably, *AtSPS1* and *AtSPS2* emerged from such a reconstruction as top co-expressors of each other, number 2 and number 4, respectively (supplemental data File 1), sharing more than half of their co-expressing genes (Fig. 2). The co-expressors of *AtSPS1* and *AtSPS2* also displayed strikingly similar patterns of subcellular distribution, including a marked prevalence for genes that encode for plastid-targeted proteins (Fig. 2). In sharp contrast, 93% of the genes that co-expressed with *AtSPS3* clustered uniquely with this enzyme (Fig. 2). Over one-third of those were found to encode for proteins targeted to the mitochondrion (Fig. 2), agreeing with the role of AtSPS3 as a ubiquinone biosynthetic enzyme in this organelle (23). Taken together, these data imply that AtSPS1 and AtSPS2 belong to the same functional network. The latter is not solely distinct from the AtSPS3 functional network but is also intimately linked to plastids. Although such a model fits with the demonstration that AtSPS2 is targeted to plastids, it conflicts with the previous assumption that AtSPS1 localizes to the endoplasmic reticulum (8, 9).

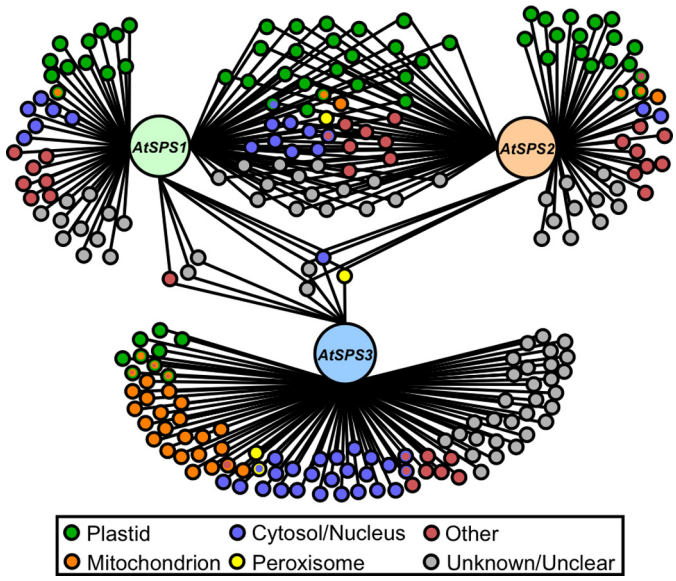

FIGURE 2. **Co-expression network of the *Arabidopsis* solanesyl-diphosphate synthase family.** The top 100 co-expressors of *AtSPS1*, *AtSPS2*, and *AtSPS3* were mined from the ATTED-II database and then aggregated using GeneVenn (29). Subcellular localization data supported by direct experimental evidence and/or manual curation were compiled from the TAIR and SUBA-2 databases. The "*other*" category regroups proteins that are located in the endoplasmic reticulum, the plasma membrane, the vacuole, or the plasmodesma or that are secreted outside of the cells.

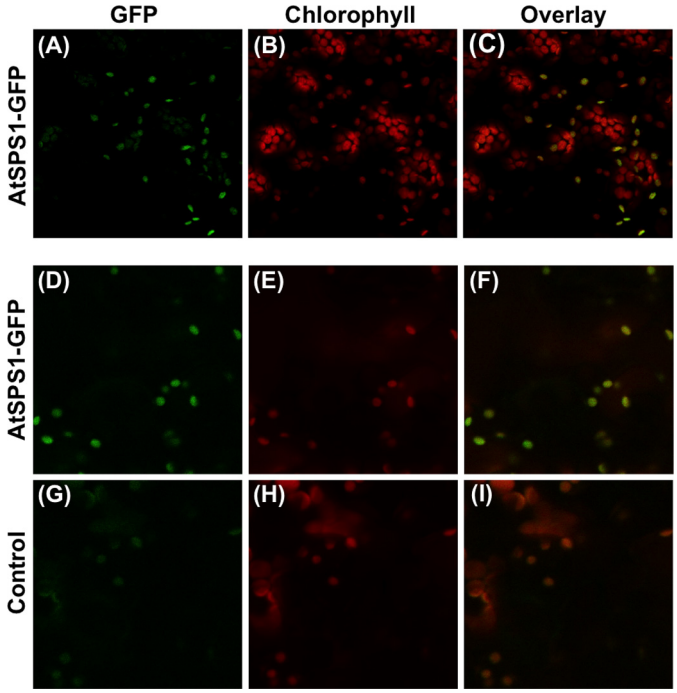

FIGURE 3. **Subcellular localization of AtSPS1.** *A–C*, transient expression of AtSPS1-GFP in tobacco leaves. *D–F*, leaf tissue of *Arabidopsis AtSPS1-GFP* transgenics. *G–I*, leaf tissue of wild type *Arabidopsis*. *A*, *D*, and *G*, *green* pseudocolor channel; *B*, *E*, and *H*, *red* pseudocolor channel; *C*, *F*, and *I*, *overlay* of *green* and *red* pseudocolor channels. Transgenics and wild type *Arabidopsis* plants were imaged with the same settings.

AtSPS1 Is Targeted Exclusively to Plastids—To reexamine the subcellular localization of AtSPS1, a 3089-bp genomic fragment comprising the *AtSPS1* sequence (minus its stop codon)

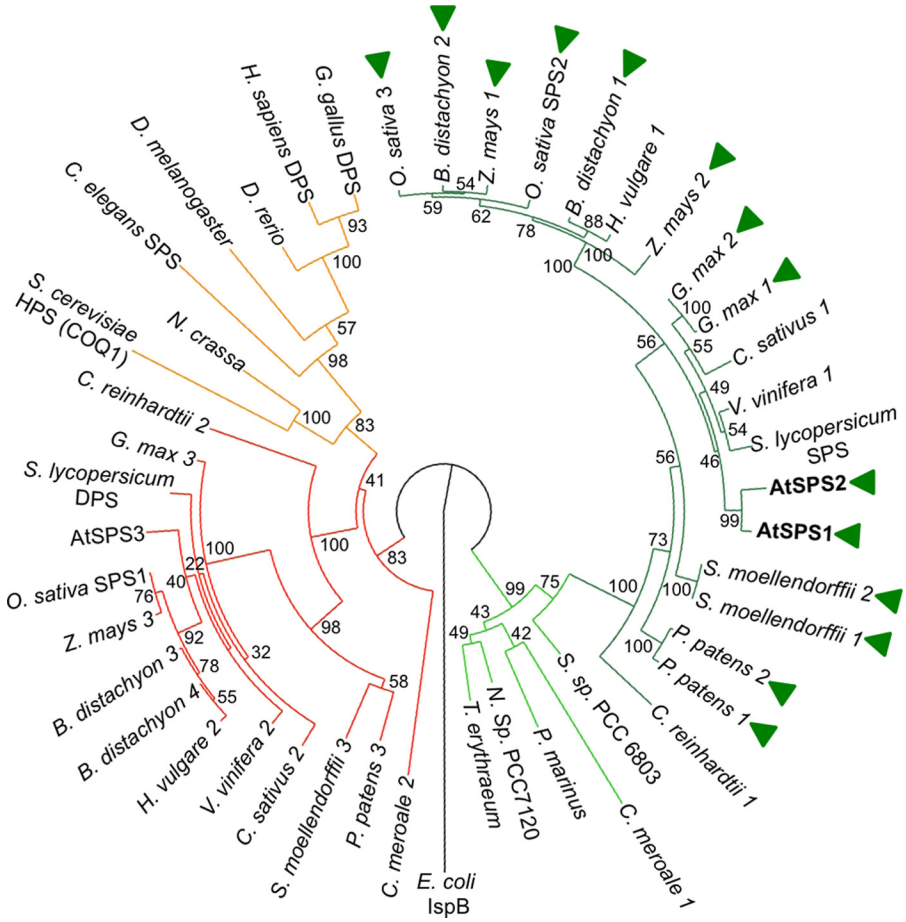

FIGURE 4. **Phylogenetic relationships of plant *trans*-long chain prenyl-diphosphate synthases to their closest relatives in prokaryotes and eukaryotes.** The closest homologs of AtSPS1 and AtSPS2 were mined from fully sequenced prokaryotic and eukaryotic genomes using BLASTp searches. Protein sequences were then processed using the following algorithm suite at Phylogeny.fr (30): MUSCLE (multiple alignment), Gblocks (curation of misalignments and divergent regions), PhyML (maximum likelihood reconstruction), and TreeDyn (tree visualization). *E. coli* octaprenyl-diphosphate synthase (IspB; YP_491372.1) served as an outgroup to root the tree. Branches of the strictly eukaryotic clade are shown in *orange* (metazoans and fungi) and *red* (plants); members of this clade are orthologous to yeast COQ1 that is targeted to the mitochondrion to make the side chain of ubiquinone. *Light green branches* mark the subfamily of cyanobacterial and plastid-encoded solanesyl-diphosphate synthases, and the *dark green branches* mark their nuclear encoded orthologs in plants; *green arrowheads* point to those that are paralogous. Bootstrap values out of 100 replications are given next to each branching. ATSPS1 (ABF58968.1), ATSPS2 (NP_173148.2), ATSPS3 (AAM13005.1), *B. distachyon* (*1*, XP_003567824.1; *2*, XP_003576903.1; *3*, XP_003563402.1; *4*, XP_003559297.1), *Caenorhabditis elegans* SPS (NP_491588.1), *C. reinhardtii* (*1*, XP_001693430.1; *2*, XP_001691069.1), *C. merolae* (*1*, NP_849058.1 plastid encoded; *2*, BAM80356.1), *Cucumis sativus* (*1*, XP_004137246.1; *2*, XP_004134571.1), *Danio rerio* (NP_001017656.1), *D. melanogaster* (NP_733425.1), *Gallus gallus* DPS (XP_418592.3), *Glycine max* (*1*, XP_003543174.1; *2*, XP_003546747.1; *3*, XP_003525839.1), *Homo sapiens* DPS (AAD28559.1), *Hordeum vulgare* (*1*, BAK00672.1; *2*, BAK05302.1), *Neurospora crassa* (XP_959949.1), *N. sp.* PCC 7120 (NP_484140.1), *Oryza sativa* (SPS1, NP_001058362.1; SPS2, Q75HZ9.2, *3*, TIGR contig TC495672), *P. patens* (*1*, XP_001775803.1; *2*, XP_001762387.1, *3*, XP_001753309.1), *Prochlorococcus marinus* (YP_001014501.1), *S. cerevisiae* HPS (EGA88084.1), *S. moellendorffii* (*1*, XP_002985427.1; *2*, XP_002979762.1; *3*, XP_002977539.1), *Solanum lycopersicum* (SPS, XP_004244308.1; DPS, NP_001234089.1), *S. sp.* PCC 6803 (NP_439899.1), *Trichodesmium erythraeum* (YP_720124.1), *Vitis vinifera* (*1*, XP_002285665.1; *2*, XP_002268229.2), *Zea mays* (*1*, ACN25661.1, *2*, NP_001149100.1, *3*, ACG33955.1). *DPS*, decaprenyl-diphosphate synthase; *HPS*, hexaprenyl-diphosphate synthase; *SPS*, solanesyl-diphosphate synthase.

as well as its 5′-untranslated region and native promoter was cloned in-frame to the 5′-end of GFP. Confocal laser scanning microscopy of the transiently expressed AtSPS1-GFP construct in tobacco leaf tissues showed a pattern of green pseudocolor that co-localized with the autofluorescence of chlorophyll in plastids (Fig. 3, *A–C*). Untransformed plastids confirmed that the fluorescence attributed to GFP was not merely due to an overflow of the red pseudocolor into the green pseudocolor channel (Fig. 3, *B* and *C*). To confirm these findings, the AtSPS1-GFP construct was introduced into *Arabidopsis* for stable expression. Imaging of the leaves of T1 transgenics demonstrated that again the fluorescence of GFP was localized in plastids (Fig. 3, *D–F*). A comparison with the leaves of wild type controls imaged at the same settings as that of the *AtSPS1-GFP* transgenics showed that the fluorescence of GFP was easily distinguishable from the background overflow of the red pseudocolor into the green channel (Fig. 3, *D–I*). These data demonstrate that when it is either transiently or stably expressed under the control of its native promoter, the AtSPS1 protein is targeted to plastids. In neither case was GFP-associated fluorescence detected outside of plastids.

Duplication of Solanesyl-diphosphate Synthase of Plastids Is Widespread in Land Plants—Database mining of fully sequenced genomes pointed to cyanobacterial *trans*-long chain prenyl-diphosphate synthases as the closest prokaryotic relatives of AtSPS1 and AtSPS2. Notably, like metazoa and fungi, cyanobacteria have only one gene coding for this class of enzymes, whereas without exception plants have several. For instance, the green alga *Chlamydomonas reinhardtii*, the red alga *Cyanidioschyzon merolae*, barley, grape, tomato, and

cucumber have two, the lycopod *Selaginella moellendorffii*, the moss *Physcomitrella patens*, corn, rice, and soybean have three like *Arabidopsis*, and the grass species *Brachypodium distachyon* have four. A maximum likelihood phylogeny showed that the plant species mentioned above generally have one of their AtSPS homologs that regroups within a strictly eukaryotic clade and one or more of the others that are monophyletic with the cyanobacterial subfamily (Fig. 4). AtSPS1, AtSPS2, and the plastid-encoded *C. merolae1* homolog, as well as tomato (SlSPS) and rice (OsSPS2) solanesyl-diphosphate synthases, both of which are targeted to plastids (10, 31), belong to this cyanobacterial lineage (Fig. 4). Importantly, the species that possess more than two *trans*-long chain prenyl-diphosphate synthases owe these extra enzymes to duplicates within the cyanobacterial/plastid subgroup (Fig. 4). The only exception is *Brachypodium*, which has duplicates in both the eukaryotic and cyanobacterial/plastid clades (Fig. 4). It thus appears that the occurrence of duplicated plastid isoforms of solanesyl-diphosphate synthase is not specific to *Arabidopsis*.

AtSPS1 and AtSPS2 Contribute to the Biosynthesis of Plastoquinone-9 and Plastochromanol-8—A T-DNA mutant corresponding to an insertion located in the first exon of *AtSPS1* (SALK_126948) was identified using the T-DNA Express gene mapping tool and confirmed by DNA genotyping (Fig. 5, *A* and *B*). RT-PCR analysis using a primer pair designed to amplify a cDNA region spanning from the end of the second exon to the beginning of the sixth exon confirmed that the *atsps1* locus was null (Fig. 5, *A* and *C*). A tandem T-DNA insertion was similarly identified in the sixth exon of *AtSPS2* (SALK_064292), but RT-PCR amplification of a cDNA region located upstream of the predicted insertion revealed that the cognate locus was not null (Fig. 5, *D–F*). Sequencing of a PCR fragment encompassing the junction between the T-DNA border and the last exon located the insertion precisely at the second nucleotide position of the *AtSPS2* stop codon (Fig. 5*D*). Conceptual translation of the cognate mRNA resulted in a chimeric protein formed from the in-frame C-terminal fusion between AtSPS2 and a T-DNA encoded polypeptide.

HPLC analyses of prenylated benzoquinones and tocochromanols showed that the content in total plastoquinone-9, quinone (oxidized) + quinol (reduced) forms, was decreased by 11 and 57% in the leaves of the *atsps1* and *atsps2* mutants, respectively, compared with that of wild type plants (Fig. 6*A*). The level of plastochromanol-8, the product of plastoquinol-9 cyclization, was decreased by about 35% in the *atsps1* plants as compared with wild type controls (Fig. 6*A*). Plastochromanol-8 was not detected in the leaves of the *atsps2* mutant (Fig. 6*A*). For each *atsps* mutant, these differences in plastoquinone-9 and plastochromanol-8 levels still strictly co-segregated with the T-DNA insertion after three back-crosses. Total tocopherol levels were either undistinguishable or, owing to a ~20% increase in α-tocopherol content, slightly higher than those of the wild type in the *atsps1* mutant and *atsps2* mutant, respectively (Fig. 6*B*). No statistically significant differences were observed in the levels of ubiquinone-9 between the mutants and the wild type control (Fig. 6*C*). Dry seeds of the *atsps1* and *atsps2* mutants accumulated 11 and 36% less plastochromanol-8 than their wild type counterparts, respectively

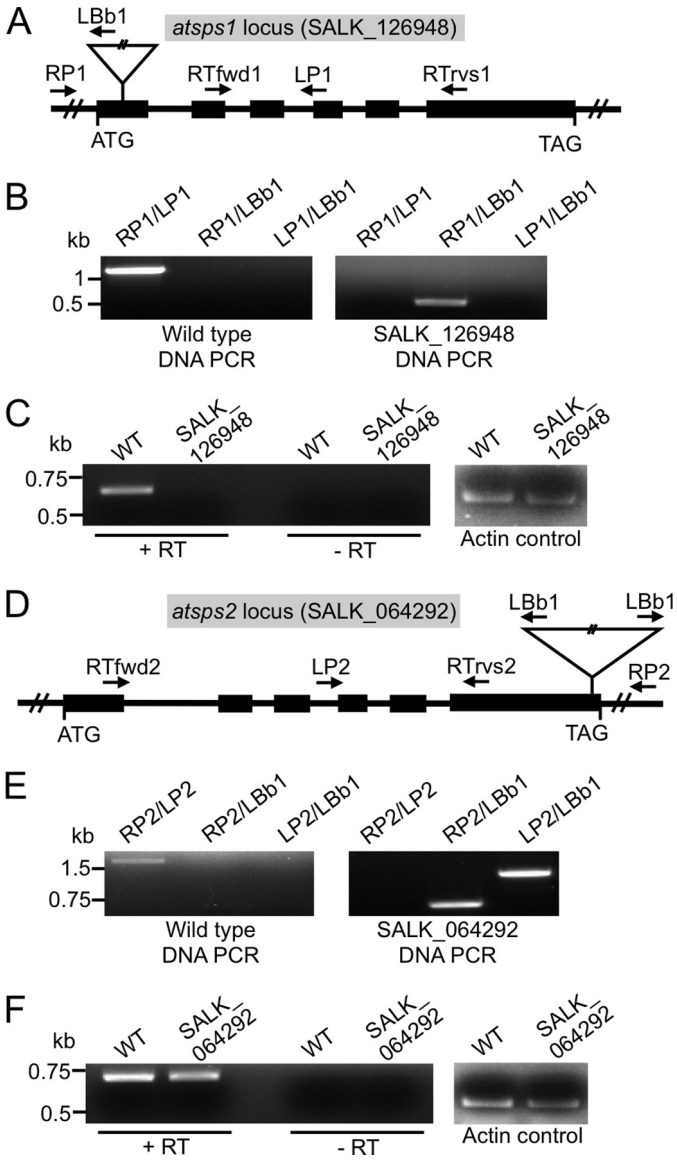

FIGURE 5. **Molecular characterization of the *atsps1* and *atsps2* T-DNA insertion mutants.** *A*, structure of the *atsps1* locus. *B*, genotyping PCR of WT *Arabidopsis* plant and *atsps1* T-DNA insertion mutant (SALK_126948). *C*, RT-PCR analyses of RNA abundance in wild type and *atsps1* plants. *D*, structure of the *atsps2* locus. *E*, genotyping PCR of WT *Arabidopsis* plant and *atsps2* T-DNA insertion mutant (SALK_064292). Note that amplifications with both RP2 and LP2 gene-specific primers in combination with the LBb1 T-DNA-specific primer in SALK_064292 mutant are diagnostic of a tandem insertion. *F*, RT-PCR analyses of RNA abundance in wild type and *atsps2* plants. *Boxes* and *lines* represent exons and introns, respectively. RP1, LP1, RP2, LP2, and LBb1 indicate the location of the genotyping primers; RTfwd1, RTrvs1, RTfwd2, and RTrvs2 indicate the location of the RT-PCR primers. −*RT*, controls for genomic DNA contamination performed without reverse transcriptase.

(Fig. 6*D*). Although *atsps2* seeds contained about 40% more α-tocopherol than wild type and *atsps1* seeds, such an increase was counterbalanced by a similar decrease in δ-tocopherol, resulting in no statistically significant difference in total tocopherol accumulation (Fig. 6*E*). The plastoquinone-9 and ubiquinone-9 levels of dry seeds were below the detection threshold. The *atsps1 atsps2* double homozygous mutant displayed a prominent albino phenotype (Fig. 7, *A* and *B*) and was devoid of plastoquinone-9 and plastochromanol-8 (Fig. 7*C*). As observed for the *atsps1* and *atsps2* single mutants, it did how-

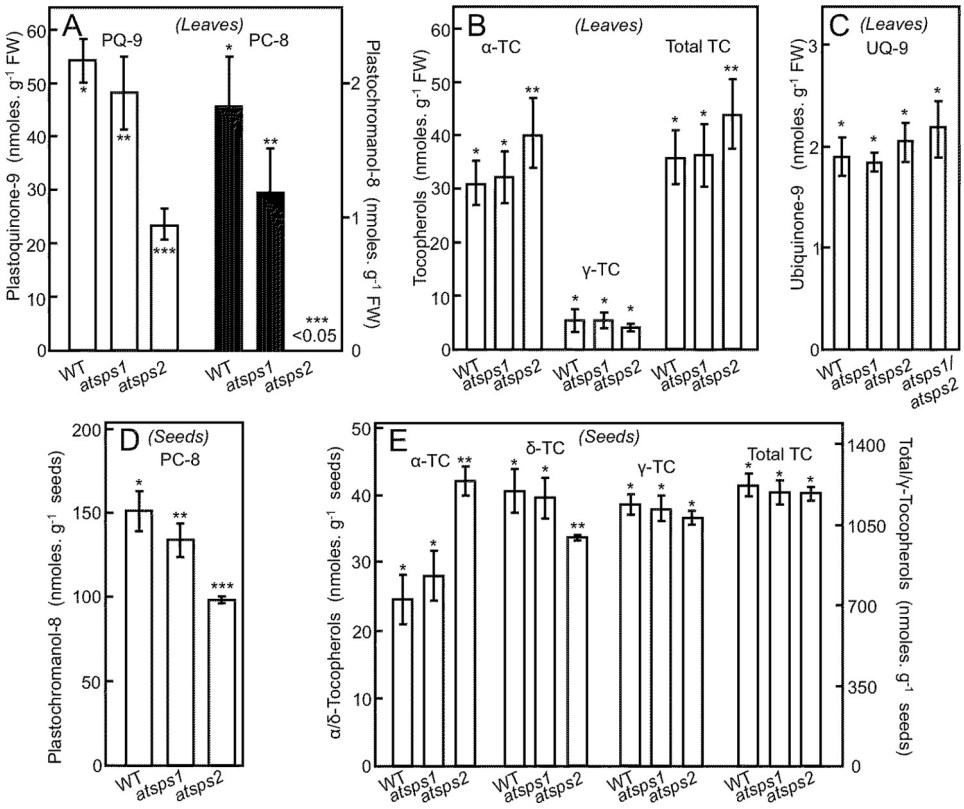

FIGURE 6. **Levels of prenylated quinones and tocochromanols in *Arabidopsis* leaves and seeds.** Extracts from leaves of 4-week-old plants grown at 120 $\mu E \cdot m^{-2} \cdot s^{-1}$ and seeds were analyzed by HPLC in spectrophotometric detection mode for plastoquinone-9 (*PQ-9*) and ubiquinone-9 (*UQ-9*) or fluorometric detection mode for plastochromanol-8 (*PC-8*) and tocopherols (α/γ-*TC*). *A*, plastoquinone-9 (*open bars*) and plastochromanol-8 (*black bars*) in leaves. *B*, α- and γ-tocopherols in leaves. *C*, ubiquinone-9 in leaves. *D*, plastochromanol-8 in seeds. *E*, tocopherols in seeds. Data are the means of 8–12 replicates ± S.E. for the measurements of plastoquinone-9, plastochromanol-8, and α- + γ-tocopherols in leaves, 5 replicates ± S.E. for that of ubiquinone-9 in the wild type and the *atsps1* and *atsps2* mutants, duplicates ± S.E. for that of ubiquinone-9 in the *atsps1/atsps2* double knock-out, and 3–6 replicates ± S.E. for plastochromanol-8 and tocopherols in seeds. Differing *asterisk* annotations indicate that the corresponding values are significantly different as determined by Fisher's least significant difference test ($p < \alpha = 0.05$) from an analysis of variance.

ever retain the ability to accumulate tocopherols to wild type levels (Fig. 7*C*). The *atsps1 atsps2* double knock-out survived *in vitro* on an external carbon source and under low illumination but never developed beyond a couple of leaves. These plants died quickly when transferred to soil, and we therefore deemed the *atsps1 atsps2* knock-out seedling-lethal. Taken together, these data indicate that AtSPS1 and AtSPS2 are involved in the biosynthesis of plastoquinone-9. Moreover, because plastoquinone-9 and plastochromanol-8 was undetectable in the *atsps1 atsps2* double homozygous mutant, it can also be deduced that the chimeric *AtSPS2* mRNA in SALK_064292 mutant (*atsps2*) is not functional. Most importantly, the deficit or absence of plastochromanol-8 in the *atsps1*, *atsps2*, and *atsps1 atsps2* knock-outs was not paralleled by that of tocopherols, as is the case for other plastochromanol-8 biosynthetic mutants (15, 12, 32). We will come back to this point later.

The Photoactive and Non-photoactive Pool Sizes of Plastoquinone-9 Are Differently Altered in the atsps1 and atsps2 Mutants—Because the quantities of plastoquinone-9 and plastochromanol-8 were altered to markedly differing extents in each *atsps* mutant, we sought to determine whether such deficiencies were related to the size of the photoactive pool of plastoquinone or to the non-photoactive one or to both. To that end, we quantified plastoquinone-9 and plastoquinol-9 in the leaves of plants placed in the dark and then exposed to saturating light intensity. In this method, the amount of plastoquinone the redox status of which responds to changes in light regime represents the size of the photoactive pool; it is calculated from the difference between the levels of plastoquinol-9 measured in the light and that measured in the dark. Conversely, the quantity of plastoquinol-9 that does not re-oxidize in the dark and that of plastoquinone-9 that is not reduced in the light represent the non-photoactive pool. These measurements showed that the pool size of photoactive plastoquinone in the *atsps1* knock-out was not statistically different from that of the wild type, whereas it was markedly decreased in the *atsps2* mutant, representing a mere 43% of the photoactive pool of control plants (Fig. 8*A*). The quantity of non-photoactive plastoquinone was decreased by 15% as compared with the wild type control in the *atsps1* mutant and by up to 60% in the *atsps2* knock-out (Fig. 8*B*). The ratio of plastoquinol-9 to plastoquinone-9 of the *atsps1* knock-out was not statistically different from that of the wild type (1.68 ± 0.51 for the WT *versus* 1.36 ± 0.20 for *atsps1*; *p* analysis of variance = 0.27). On the other hand, this ratio was significantly lower in the *atsps2* knock-out (0.80 ± 0.19; *p* analysis of variance = 0.003), indicating that the redox state of non-photoactive plastoquinone had been altered in these plants. It should be noted that the *atsps1* knock-out, in which the deficit of plastoquinone-9 has an impact solely on its non-photoactive

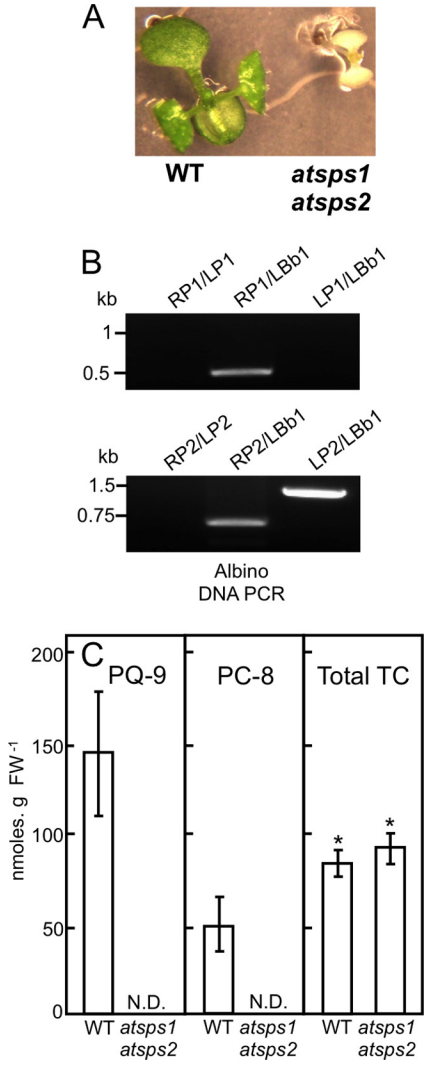

FIGURE 7. **The *atsps1 atsps2* double homozygous mutant is devoid of plastoquinone-9 and plastochromanol-8.** *A*, phenotype comparison between WT and *atsps1 atsps2* double homozygous mutant plants. Three-week-old seedlings from the *atsps1* × *atsps2* F2 segregating progeny were grown at 120 $\mu E \cdot m^{-2} \cdot s^{-1}$ on Murashige and Skoog solid medium. *B*, genotyping PCR of wild type *Arabidopsis* and *atsps1 atsps2* double homozygous mutant plants. Primer pairs were the same as those described in the legend for Fig. 5. *C*, plastoquinone-9 (*PQ-9*), plastochromanol-8 (*PC-8*), and tocopherol (*TC*) content in the cotyledons of wild type and *atsps1 atsps2* double homozygous mutant plants. *N.D.*, not detected.

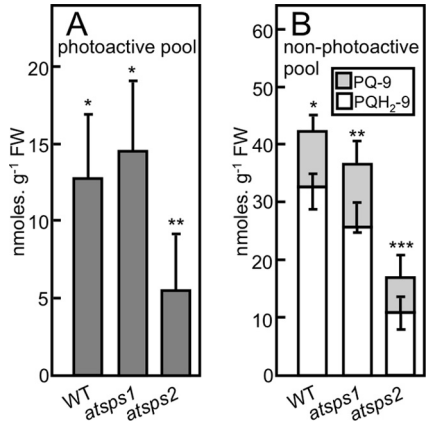

FIGURE 8. **Quantification of the photoactive and non-photoactive pool sizes of plastoquinone-9 in *Arabidopsis* leaves.** *A*, photoactive pool. The quantity of plastoquinol-9 was first determined in the leaves of plants that had been kept in the dark for at least 2 h. Plastoquinol-9 was then requantified after the plants had been exposed to high light intensity (1100 $\mu E \cdot m^{-2} \cdot s^{-1}$) for 5 min. The size of the photoactive pool of plastoquinone-9 was calculated by subtracting the amount of plastoquinol-9 measured in the light from that measured in the dark. *B*, non-photoactive pools of plastoquinol-9 (*PQH_2-9*, not reoxidized in the dark) and plastoquinone-9 (*PQ-9*, not reduced in the light). Data are the means of 4–6 replicates ± S.E. Differing *asterisk* annotations next to each *error bar* indicate that the corresponding values are significantly different as determined by Fisher's least significant difference test ($p < \alpha = 0.05$) from an analysis of variance.

pool, also displays a marked decrease in plastochromanol-8 content.

The atsps2 Knock-out Displays a Severe Increase in Photoinhibition at High Light Intensity—Whereas on Murashige and Skoog solid medium containing sucrose and under a moderate light regime, the *atsps1* and *atsps2* knock-outs were morphologically indistinguishable from the wild type (data not shown), when grown on soil the *atsps2* knock-out seemed to develop more slowly than the *atsps1* knock-out and the wild type (Fig. 9*A*). At a high light regime, the *atsps2* mutant displayed a remarkably stunted phenotype and pale yellowish leaves, indicative of a strong increase in photosensitivity (Fig. 9*B*). Analyses of the induction of chlorophyll *a* fluorescence showed that wild type and *atsps* plants grown at moderate light intensity (120 $\mu E \cdot m^{-2} \cdot s^{-1}$) displayed overall similar photosynthetic performances (Fig. 9*C*). Maximum quantum efficiencies (F_v/F_m) of photosystem II were typical of non-stressed *Arabidopsis* leaves (33), ranging from 0.77 for the wild type to 0.76 and 0.75 for the *atsps1* and *atsps2* knock-outs, respectively (Fig. 9*C* and Table 1). Similarly, calculations of the variable fluorescence decrease ratio (R_{fd}), which correlates linearly with net CO_2 assimilation and assesses potential photosynthetic activity (34), did not reveal any defects for either of the *atsps* mutants (Table 1). Somewhat lower values for NPQ, *i.e.* the protective dissipation of excess chlorophyll excitation as heat (35), were observed for both mutants (Table 1). Upon exposure to high light intensity (800 $\mu E \cdot m^{-2} \cdot s^{-1}$), however, the fluorescence emission of the *atsps2* knock-out differed noticeably from that of the *atsps1* mutant and wild type control (Fig. 9, *D–F*). The F_v/F_m, R_{fd}, and NPQ values of the *atsps2* mutant collapsed after only 2 h of strong illumination (Table 1). Already at this point, photoinhibition, *i.e.* the irreversible loss of photosystem II efficiency, was five times higher in the *atsps2* mutant than in the *atsps1* and wild type plants (Table 1). By 24 h of high light treatment, the F_v/F_m value of the *atsps2* knock-out had dropped to 0.31, pointing to a critical defect of photosystem II, and by 48 h of treatment all of the fluorescence parameters indicated that photosynthesis was barely operating (Table 1). It is noteworthy that up until 48 h of exposure to high light intensity, NPQ was the sole calculated fluorescence parameter that differed markedly between the *atsps1* mutant and the wild type (Table 1). Thus, this observation provides evidence that non-photoactive plastoquinone-9, the pool of which is altered independently of that of its photoactive counterpart in the *atsps1* knock-out (Fig. 8*B*), is involved in NPQ. Immunodetection of the reaction center polypeptide D1 showed that photoinhibition of the *atsps2* knock-out at high light intensity was paralleled by a loss of the core of photosystem II complex (Fig. 9*G*). In contrast, measurements of P700 absorption indicated that the photo-oxidation of

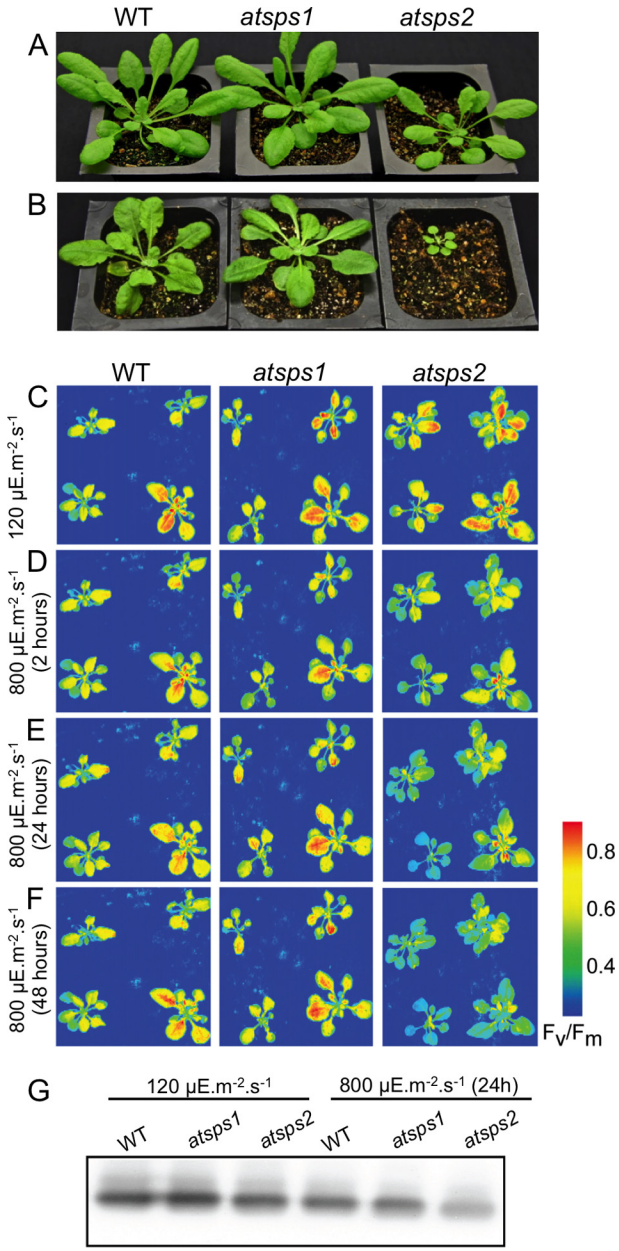

FIGURE 9. **Phenotypes and analysis of photosystem II of wild type, *atsps1*, and *atsps2* plants.** *A*, 1-month-old plants grown at 110 $\mu E \cdot m^{-2} \cdot s^{-1}$ for 16-h days. *B*, 1-month-old plants grown at 500 $\mu E \cdot m^{-2} \cdot s^{-1}$ for 16-h days. *C*, imaging of maximum quantum efficiency (F_v/F_m) of photosystem II of wild type, *atsps1*, and *atsps2* plants grown at moderate light intensity (120 $\mu E \cdot m^{-2} \cdot s^{-1}$). *D–F*, representative FluorCam 700 MF images acquired after the plants had been exposed to high light intensity (800 $\mu E \cdot m^{-2} \cdot s^{-1}$) for 2, 24, and 48 h, respectively. Plants were dark-adapted for 20 min prior to illumination with actinic light. *G*, immunodetection of photosystem II polypeptide D1 in thylakoid membranes prepared from wild type, *atsps1*, and *atsps2* plants grown at moderate light intensity (120 $\mu E \cdot m^{-2} \cdot s^{-1}$) or exposed to high light regime (800 $\mu E \cdot m^{-2} \cdot s^{-1}$) for 24 h. Each of the *lanes* contains 20 μg of proteins.

photosystem I in the *atsps2* mutant was only marginally lower than that of the *atsps1* knock-out and wild type control, under either a normal or high light regime (Fig. 10, *A* and *B*). Immunodetection of the photosystem I subunit PsaA did not reveal any significant differences between the *atsps* mutants and the wild type (Fig. 10*C*). Altogether, these data indicate that the bulk of the photodamage in the *atsps2* knock-out was specific to photosystem II. In a parallel experiment designed to compare

TABLE 1

Calculated fluorescence parameters of wild type, *atsps1*, and *atsps2* plants

Values of maximum quantum efficiency of photosystem II (F_v/F_m), variable fluorescence decrease ratio (R_{fd}), NPQ, and percentages of photoinhibition were calculated based on fluorescence measurements like those shown in Fig. 11. Data are means of 20 measurements ± S.D.

Fluorescence parameters	WT	*atsps1*	*atsps2*
120 $\mu E \cdot m^{-2} \cdot s^{-1}$			
F_v/F_m	0.77 ± 0.01	0.76 ± 0.01	0.75 ± 0.03
R_{fd}	2.12 ± 0.06	2.31 ± 0.03	2.11 ± 0.02
NPQ	1.24 ± 0.02	1.08 ± 0.02	1.12 ± 0.01
800 $\mu E \cdot m^{-2} \cdot s^{-1}$ (2 h)			
F_v/F_m	0.75 ± 0.02	0.74 ± 0.02	0.64 ± 0.02
R_{fd}	1.85 ± 0.04	1.65 ± 0.05	1.23 ± 0.03
NPQ	1.63 ± 0.03	1.42 ± 0.03	0.97 ± 0.02
Photoinhibition (%)	3.0 ± 2.1	3.2 ± 2.4	15 ± 3.7
800 $\mu E \cdot m^{-2} \cdot s^{-1}$ (24 h)			
F_v/F_m	0.72 ± 0.04	0.70 ± 0.05	0.31 ± 0.05
R_{fd}	1.61 ± 0.07	1.44 ± 0.05	0.32 ± 0.03
NPQ	1.43 ± 0.03	0.87 ± 0.03	0.52 ± 0.03
Photoinhibition (%)	6.5 ± 3.3	7.9 ± 3.4	59 ± 17.2
800 $\mu E \cdot m^{-2} \cdot s^{-1}$ (48 h)			
F_v/F_m	0.71 ± 0.03	0.62 ± 0.04	0.15 ± 0.07
R_{fd}	1.42 ± 0.08	1.24 ± 0.07	0.21 ± 0.03
NPQ	1.21 ± 0.05	0.83 ± 0.05	0.41 ± 0.07
Photoinhibition (%)	7.9 ± 3.8	18.5 ± 5.3	80 ± 27.4

the plastoquinone-9 and tocochromanol levels of the wild type and *atsps* mutants during their acclimation to high light conditions, plants were pregrown under a moderate light regime (110 $\mu E \cdot m^{-2} \cdot s^{-1}$) with alternating day and night cycles (16-h days) and then exposed to continuous high light intensity (600 $\mu E \cdot m^{-2} \cdot s^{-1}$) for 48 h. Once switched to high light, the wild type and *atsps1* plants both displayed a linear increase in plastoquinone-9 levels, although the rate of accumulation was comparatively half as fast in the mutant (Fig. 11*A*). Notably, in the wild type plants the accumulation of plastoquinone-9 coincided with an increase in the level of *AtSPS1* and *AtSPS2* transcripts (Fig. 11*A*, *inset*). Meanwhile the quantity of plastoquinone-9 in the *atsps2* mutant steadily decreased and after 48 h was only half of its value at the onset of the high light treatment (Fig. 11*A*). Plastochromanol-8 levels decreased at a rate of 1.9 and 1.5 $nmol \cdot g^{-1}$ fresh weight/24 h in the wild type control and *atsps1* mutant, respectively, while remaining below the detection limit in the *atsps2* mutant (Fig. 11*B*). As for tocopherols, the quantity of which is known to increase dramatically in leaves exposed to high light intensities (36), no significant differences in the rate of accumulation was observed between the *atsps* mutants and the wild type control (Fig. 11*C*).

The Absence of Plastochromanol-8 Does Not Alter Seed Longevity in the atsps1 atsps2 Double Knock-out—Having shown that the *atsps* mutants accumulated tocopherols to wild type levels, we investigated how in this context a deficit in antioxidant activity restricted to that of plastochromanol-8 would impact seed longevity. As the duration of desiccation and storage had been shown to be key determinants for the germination of tocochromanol biosynthetic mutants in *Arabidopsis* (15), tests of accelerated aging were performed on F2 seeds resulting from the cross between the homozygous *atsps1* and *atsps2* mutants. All segregating genotypes were therefore rigorously harvested at the same time and subjected to the same treatments. Surprisingly, the germination rates of both the aged and non-aged populations were similar, and the cognate seedlings

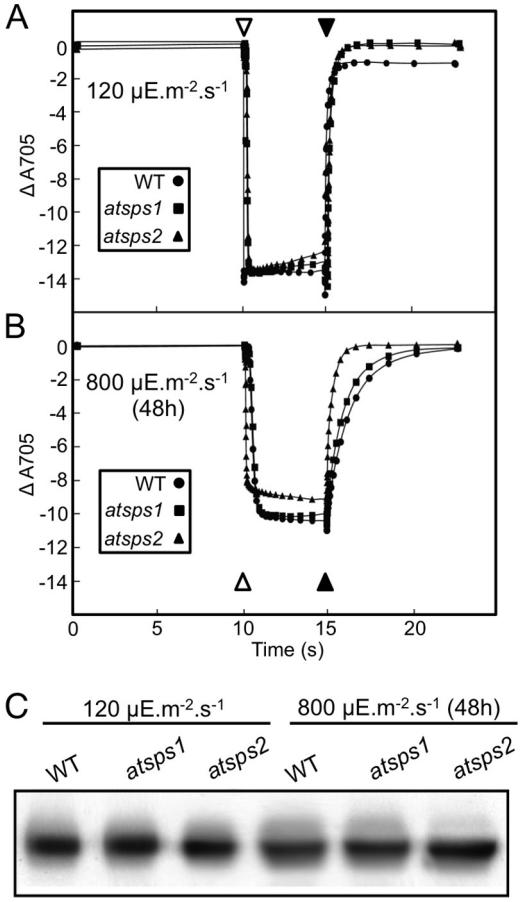

FIGURE 10. **Analysis of photosystem I of wild type, *atsps1*, and *atsps2* plants.** *A* and *B*, representative kinetics of change in absorbance during photooxidation of P700 in the leaves of wild type, *atsps1*, and *atsps2* plants grown at moderate light intensity (120 μE·m^{-2}·s^{-1}) or exposed to high light regime (800 μE·m^{-2}·s^{-1}) for 48 h. *Open* and *filled arrowheads* indicate the start and end of far-red illumination, respectively. Leaves were dark-adapted for 20 min and then preilluminated with far-red light for 2 min prior to the measurements. *C*, immunodetection of photosystem I subunit PsaA in thylakoid membranes prepared from wild type, *atsps1*, and *atsps2* plants grown at moderate light intensity (120 μE·m^{-2}·s^{-1}) or exposed to high light regime (800 μE·m^{-2}·s^{-1}) for 48 h. Each of the *lanes* contained 20 μg of proteins.

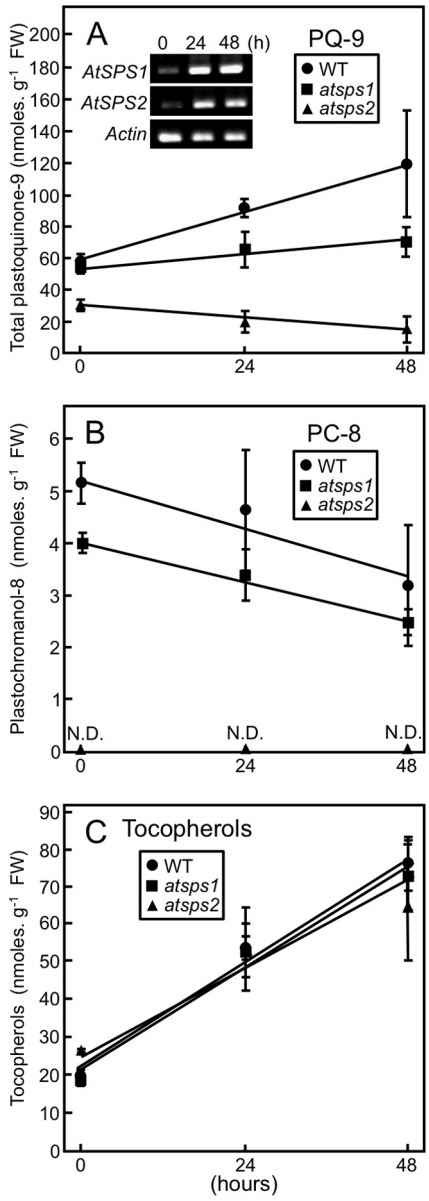

FIGURE 11. **Plastoquinone-9 and tocochromanol levels of *Arabidopsis* leaves during acclimation to high light intensity.** Three-week-old wild type, *atsps1*, and *atsps2* plants grown at moderate light intensity (110 μE·m^{-2}·s^{-1}; 16-h days) were exposed to continuous high light (600 μE·m^{-2}·s^{-1}) for 48 h. Rosette leaves were sampled just before the switch to high light and then at 24 and 48 h after. *A*, plastoquinone-9; *B*, plastochromanol-8; *C*, total tocopherols. The *inset* in *A* shows the RT-PCR analyses of RNA abundance for *AtSPS1*, *AtSPS2*, and the actin control in the leaves of the wild type.

segregated according to the ratios expected for two unlinked genes in canonical Mendelian inheritance (Table 2). Such a finding was particularly remarkable in the case of the double *atsps1 atsps2* knock-outs, indicating that the absence of plastochromanol-8 had no visible impact on seed longevity and germination. Neither the seedlings of the double *atsps1 atsps2* knock-out nor those of its *atsps* parents exhibited the failure to expand cotyledons that is typically associated with tocochromanol deficiencies (data not shown). None of the aged *vte2-1* mutant seeds, which are devoid of tocopherols and display a marked decrease in longevity (20), germinated, thus verifying the efficiency of the aging procedure in our hands (Table 2).

DISCUSSION

Confusion has long prevailed regarding the identity of the *Arabidopsis* solanesyl-diphosphate synthase that makes the side chain of plastoquinone-9. The corresponding activity was initially attributed to gene *At1g78510* (*AtSPS1*) and then to gene *At1g17050* (*AtSPS2*), whereas *AtSPS1* was reassigned to the biosynthesis of the ubiquinone-9 side chain (8, 9, 27). Further complicating the picture, a third *trans*-long chain prenyl-diphosphate synthase, the product of gene *At2g34630* (*AtSPS3*), was recently identified in *Arabidopsis* and shown to be capable of producing solanesyl diphosphate (28). Nevertheless, direct evidence of function in plants was missing all along, leading to the common belief that each of these three enzymes could function in the biosynthesis of both plastoquinone-9 and ubiquinone-9 (27, 28, 37).

Functional modeling shows that *AtSPS1* and *AtSPS2* are linked with each other as well as with plastid metabolism, whereas *AtSPS3* is a marked outlier. Coinciding with these findings, AtSPS1 and AtSPS2 both displayed canonical plastid pre-

sequences (Fig. 12), and previous studies have indeed confirmed that AtSPS2 is targeted exclusively to chloroplasts (8, 9, 38, 39). The localization of GFP-fused proteins demonstrates that this strict plastid localization holds true for AtSPS1 as long as the cognate gene is expressed under the control of its native promoter.

Our data show that the *atsps1* and *atsps2* knock-outs both display lower levels of plastoquinone-9. The fact that the *atsps1 atsps2* double knock-out is devoid of plastoquinone-9 and cannot grow photoautotrophically rules out that an additional *trans*-long chain prenyl-diphosphate synthase contributes to the biosynthesis of plastoquinone-9. Importantly, the absence of AtSPS1 and AtSPS2 does not impact the level of ubiquinone-9. This result is supported by the observation that in tomato the *trans*-long chain prenyl-diphosphate synthases that elongate the allylic diphosphate precursors of ubiquinone-10 and plastoquinone-9, respectively, cannot complement the silencing of each other (31). The correct functional assignment of the *AtSPS* members is therefore as follows. (i) AtSPS1 and AtSPS2 contribute exclusively to the biosynthesis of plastoquinone-9. The corresponding genes descend from cyanobacteria and are most probably in-paralogs, *i.e.* originate from a gene duplication event that postdates the speciation of *Arabidopsis*. Similar duplications of solanesyl-diphosphate synthase occurred multiple times throughout terrestrial plant lineages resulting in in-paralogs that have been readily mistaken in most genomic databases for the *trans*-long prenyl-diphosphate synthases required for the biosynthesis of ubiquinone. (ii) AtSPS3 is dedicated to the biosynthesis of ubiquinone-9, being part of a distinct phylogenetic clade that regroups COQ1-type proteins from other eukaryotic organisms, photosynthetic or not.

It is evident from our data that AtSPS2 bears most of the plastoquinone-9 biosynthetic flux. The *atsps2* knock-out lacks close to two-thirds of its photoactive and non-photoactive pools of plastoquinone-9, and exposure to high light exacerbates the deficit, leading to specific and irreversible damage to photosystem II. Although comparatively small, the loss of plastoquinone-9 in the *atsps1* knock-out is remarkable, for it is restricted to the non-photoactive pool and is sufficient to wipe out about half of the plastochromanol-8 content of leaves. Thus, two notable features of the architecture of plastochromanol-8 biosynthesis in photosynthetic tissues emerged from these observations. First, plastochromanol-8 originates predominantly, if not exclusively, from the non-photoactive pool of plastoquinone-9, agreeing with the co-occurrence of three plastochromanol-8 biosynthetic enzymes, NAD(P)H quinone oxidoreductase C1, tocopherol cyclase, and ABC1-like kinase, in plastoglobules (Fig. 1) (13, 40–43). Second, only a fraction of non-photoactive plastoquinol-9 is cyclized into plastochromanol-8. The leaves of the *atsps2* mutant, in which plastochromanol-8 is undetectable while the standing pool of non-photoactive plastoquinol-9 still represents three times the quantity of

TABLE 2

Segregation ratios of the *atsps1* × *atsps2* F2 population

Three-month-old seeds were subjected to accelerated aging and then vernalized, whereas control seeds were vernalized without prior aging treatment. Aged and control seeds were then allowed to germinate on Murashige and Skoog solid medium containing sucrose in 16-h days (110 $\mu E \cdot m^{-2} \cdot s^{-1}$) at 22 °C. Germinated plants were scored and genotyped after 3 weeks. Numbers of plants calculated from the Mendelian segregation ratios are shown in parentheses.

Plants	Number of plants			
	Control	*(Expected)*	*Aged*	*(Expected)*
Genotype				
AtSPS1/AtSPS1; AtSPS2/AtSPS2	13	(13)	15	(17)
AtSPS1/AtSPS1; atsps2/AtSPS2	29	(26)	32	(33)
atsps1/AtSPS1; AtSPS2/AtSPS2	24	(26)	28	(33)
atsps1/AtSPS1; atsps2/AtSPS2	53	(52)	75	(67)
atsps1/AtSPS1; atsps2/atsps2	21	(26)	34	(33)
atsps1/atsps1; atsps2/AtSPS2	24	(26)	23	(33)
atsps1/atsps1; AtSPS2/AtSPS2	16	(13)	15	(17)
AtSPS1/AtSPS1; atsps2/atsps2	12	(13)	22	(17)
atsps1/atsps1; atsps2/atsps2	15	(13)	18	(17)
Not germinated	1		5	
Total	208	(208)	267	(267)
Aging treatment control				
vte2-1/vte2-1	77		138	
Not germinated	3		138	

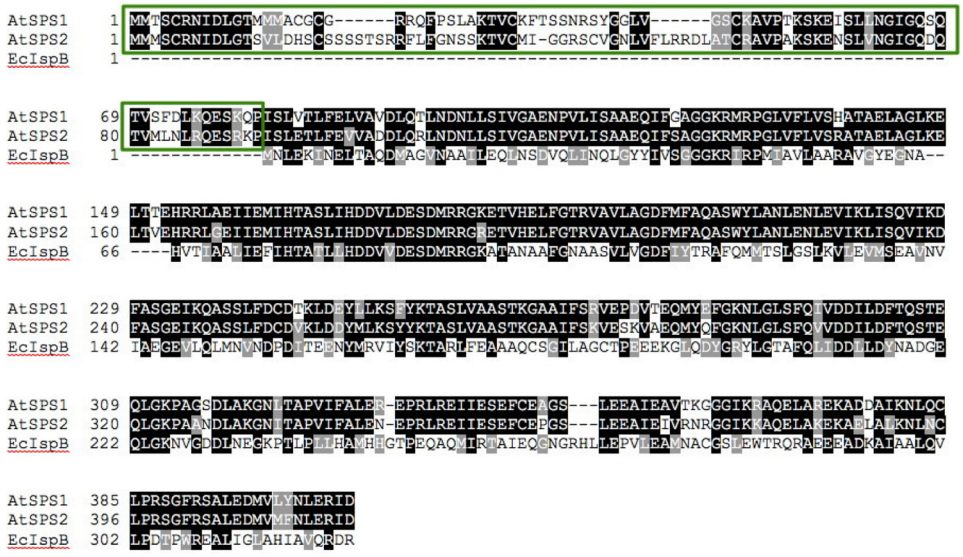

FIGURE 12. **Sequence alignment of AtSPS1 (ABF58968) and AtSPS2 (NP_173148) with their octaprenyl-diphosphate synthase homologue in *E. coli* (EcIspB; YP_491372).** Note the N-terminal extensions of the plant enzymes (in *green boxes*) as predicted by both WoLF PSORT and TargetP 1.1 to encode plastid targeting peptides. AtSPS1 and AtSPS2 share 80% identical residues, pointing to a recent gene duplication. Identical residues are *shaded* in *black* and similar ones in *gray*. *Dashes* symbolize gaps introduced to maximize alignment.

plastochromanol-8 of wild type plants, exemplifies the most extreme case of such an arrangement. Our data show that this low level of cyclization does not result from a side effect of the loss of plastoquinone-9 on tocopherol cyclase activity, for the *atsps1 atsps2* double mutant, as well as its *atsps* parents, accumulates tocopherols to wild type levels. We propose instead that the access of tocopherol cyclase to plastoquinol-9 is restricted severely in plastoglobules, possibly in a fashion similar to the protein crowding that hinders the diffusion of plastoquinone-9 molecules in thylakoid membranes (44). In support of such a scenario, there is mounting evidence that plastoglobules are not mere depot sites for lipids as thought initially, but are authentic plastidial subcompartments derived from thylakoid membranes and associated with many enzymes and structural proteins (41, 45, 46).

Although the occurrence of plastochromanol-8 in plant tissues has been known for almost 5 decades, its physiological significance is particularly unclear. On the one hand, the genetic dissection of tocochromanol biosynthesis in *Arabidopsis* demonstrates that the presence of plastochromanol-8 in the seeds of tocopherol-deficient mutants mitigates oxidative damage to lipids and its subsequent negative effects on germination (15). On the other hand, one could argue that the occurrence of plastochromanol-8 in seeds that are devoid of tocopherols does not *a priori* occur in wild type plants. It appears instead that the amount of tocopherol in seeds dwarfs that of plastochromanol-8. Thus, calculations from our data and those of others (15, 12) show that the pool size of plastochromanol-8 in *Arabidopsis* seeds ranges from a mere 8 to 13 mol % of that of tocopherols, with even a report of a value as low as 1 mol % (32). Our data demonstrate that, without loss of tocopherols, plastochromanol-8 is not essential for seed survival and germination and therefore invite the question of whether the cyclization of plastoquinol-9 in seeds could simply represent a side-reaction of the accumulation of tocopherols. Along this line, it is noteworthy that hydroxyplastochromanol-8, the main oxidation product of plastochromanol-8, is undetectable in *Arabidopsis* seeds (14). Arguably, the situation might be different in other organs. In particular, there is evidence that the levels of plastochromanol-8 and hydroxyplastochromanol-8 in leaves increase substantially during aging and can total up to three-quarters of the molar amount of α-tocopherol (14). It is not possible from our data, however, to verify the existence of a photoprotective role of plastochromanol-8, for the leaves of the *atsps* mutants also display lower levels of plastoquinol-9, itself an antioxidant in thylakoids and a necessary redox cofactor for the biosynthesis of carotenoids (3, 47). Lastly, in connection with the current enigma of how changes in the redox state of plastoquinone-9 modulate gene expression in plastids and the nucleus (5), the *atsps1* and *atsps2* knock-outs might be invaluable tools to probe the respective contribution of the photoactive and non-photoactive pools of plastoquinone-9 to redox sensing and signaling.

Acknowledgments—We thank Dr. E. Cahoon for the gift of the vte-2-1 seeds, Hardik Kundariya for generating the Arabidopsis atsps1 atsps2 double knock-out, and Dr. A. L. Ducluzeau for taking the pictures of the Arabidopsis plants.

REFERENCES

1. Nelson, N., and Yocum, C. F. (2006) Structure and function of photosystems I and II. *Annu. Rev. Plant Biol.* **57,** 521–565
2. Cooley, J. W., and Vermaas, W. F. (2001) Succinate dehydrogenase and other respiratory pathways in thylakoid membranes of *Synechocystis* sp. strain PCC 6803: capacity comparisons and physiological function. *J. Bacteriol.* **183,** 4251–4258
3. Norris, S. R., Barrette, T. R., and DellaPenna, D. (1995) Genetic dissection of carotenoid synthesis in *Arabidopsis* defines plastoquinone as an essential component of phytoene desaturation. *Plant Cell* **7,** 2139–2149
4. Mullineaux, C. W., and Emlyn-Jones, D. (2005) State transitions: an example of acclimation to low-light stress. *J. Exp. Bot.* **56,** 389–393
5. Rochaix, J. D. (2013) Redox regulation of thylakoid protein kinases and photosynthetic gene expression. *Antioxid. Redox Signal.* **18,** 2184–2201
6. Norris, S. R., Shen, X., and DellaPenna, D. (1998) Complementation of the *Arabidopsis pds1* mutation with the gene encoding *p*-hydroxyphenylpyruvate dioxygenase. *Plant Physiol.* **117,** 1317–1323
7. Sadre, R., Frentzen, M., Saeed, M., and Hawkes, T. (2010) Catalytic reactions of the homogentisate prenyl-transferase involved in plastoquinone-9 biosynthesis. *J. Biol. Chem.* **285,** 18191–18198
8. Jun, L., Saiki, R., Tatsumi, K., Nakagawa, T., and Kawamukai, M. (2004) Identification and subcellular localization of two solanesyl diphosphate synthases from *Arabidopsis thaliana*. *Plant Cell Physiol.* **45,** 1882–1888
9. Hirooka, K., Izumi, Y., An, C. I., Nakazawa, Y., Fukusaki, E., and Kobayashi, A. (2005) Functional analysis of two solanesyl diphosphate synthases from *Arabidopsis thaliana*. *Biosci. Biotechnol. Biochem.* **69,** 592–601
10. Ohara, K., Sasaki, K., and Yazaki, K. (2010) Two solanesyl diphosphate synthases with different subcellular localizations and their respective physiological roles in *Oryza sativa*. *J. Exp. Bot.* **61,** 2683–2692
11. Cheng, Z., Sattler, S., Maeda, H., Sakuragi, Y., Bryant, D. A., and DellaPenna, D. (2003) Highly divergent methyltransferases catalyze a conserved reaction in tocopherol and plastoquinone synthesis in cyanobacteria and photosynthetic eukaryotes. *Plant Cell* **15,** 2343–2356
12. Szymańska, R., and Kruk, J. (2010) Plastoquinol is the main prenyllipid synthesized during acclimation to high light conditions in *Arabidopsis* and is converted to plastochromanol by tocopherol cyclase. *Plant Cell Physiol.* **51,** 537–545
13. Eugeni Piller, L., Besagni, C., Ksas, B., Rumeau, D., Bréhélin, C., Glauser, G., Kessler, F., and Havaux, M. (2011) Chloroplast lipid droplet type II NAD(P)H quinone oxidoreductase is essential for prenylquinone metabolism and vitamin K_1 accumulation. *Proc. Natl. Acad. Sci. U.S.A.* **108,** 14354–14359
14. Szymańska, R., and Kruk, J. (2010) Identification of hydroxyl-plastochromanol in *Arabidopsis* leaves. *Acta Biochim. Pol.* **57,** 105–108
15. Mène-Saffrané, L., Jones, A. D., and DellaPenna, D. (2010) Plastochromanol-8 and tocopherols are essential lipid-soluble antioxidants during seed desiccation and quiescence in *Arabidopsis*. *Proc. Natl. Acad. Sci. U.S.A.* **107,** 17815–17820
16. Tian, L., DellaPenna, D., and Dixon, R. A. (2007) The *pds2* mutation is a lesion in the *Arabidopsis* homogentisate solanesyltransferase gene involved in plastoquinone biosynthesis. *Planta* **226,** 1067–1073
17. Dawson, R. M. C., Elliot, D. C., Elliot, W. H., and Jones, K. M. (1986) *Data for Biochemical Research*, (Dawson, R. M. C., ed) 3rd Ed., pp. 132, 138, Oxford University Press, New York
18. Leerbeck, E., Sondergaard, E., and Dam, H. (1967) Occurrence of a plastochromanol in linseed oil. *Acta Chem. Scand.* **21,** 2582
19. Alonso, J. M., Stepanova, A. N., Leisse, T. J., Kim, C. J., Chen, H., Shinn, P., Stevenson, D. K., Zimmerman, J., Barajas, P., Cheuk, R., Gadrinab, C., Heller, C., Jeske, A., Koesema, E., Meyers, C. C., Parker, H., Prednis, L., Ansari, Y., Choy, N., Deen, H., Geralt, M., Hazari, N., Hom, E., Karnes, M., Mulholland, C., Ndubaku, R., Schmidt, I., Guzman, P., Aguilar-Henonin, L., Schmid, M., Weigel, D., Carter, D. E., Marchand, T., Risseeuw, E., Brogden, D., Zeko, A., Crosby, W. L., Berry, C. C., and Ecker, J. R. (2003) Genome-wide insertional mutagenesis of *Arabidopsis thaliana*. *Science* **301,** 653–657
20. Sattler, S. E., Gilliland, L. U., Magallanes-Lundback, M., Pollard, M., and DellaPenna, D. (2004) Vitamin E is essential for seed longevity and for pre-

venting lipid peroxidation during germination. *Plant Cell* **16,** 1419–1432
21. Christensen, A. C., Lyznik, A., Mohammed, S., Elowsky, C. G., Elo, A., Yule, R., and Mackenzie, S. A. (2005) Dual-domain, dual-targeting organellar protein presequences in *Arabidopsis* can use non-AUG start codons. *Plant Cell* **17,** 2805–2816
22. Clough, S.J., and Bent, A.F. (1998) Floral dip: a simplified method for *Agrobacterium*-mediated transformation of *Arabidopsis thaliana*. *Plant J.* **16,** 735–743
23. Ducluzeau, A. L., Wamboldt, Y., Elowsky, C. G., Mackenzie, S. A., Schuurink, R. C., and Basset, G. J. (2012) Gene network reconstruction identifies the authentic *trans*-prenyl-diphosphate synthase that makes the solanesyl moiety of ubiquinone-9 in *Arabidopsis*. *Plant J.* **69,** 366–375
24. Fristedt, R., Willig, A., Granath, P., Crèvecoeur, M., Rochaix, J. D., and Vener, A.V. (2009) Phosphorylation of photosystem II controls functional macroscopic folding of photosynthetic membranes in *Arabidopsis*. *Plant Cell* **21,** 3950–3964
25. Asai, K., Fujisaki, S., Nishimura, Y., Nishino, T., Okada, K., Nakagawa, T., Kawamukai, M., and Matsuda, H. (1994) The identification of *Escherichia coli ispB* (cel) gene encoding the octaprenyl diphosphate synthase. *Biochem. Biophys. Res. Commun.* **202,** 340–345
26. Ashby, M. N., and Edwards, P. A. (1990) Elucidation of the deficiency in two yeast coenzyme Q mutants. Characterization of the structural gene encoding hexaprenyl pyrophosphate synthetase. *J. Biol. Chem.* **265,** 13157–13164
27. Hirooka, K., Bamba, T., Fukusaki, E., and Kobayashi, A. (2003) Cloning and kinetic characterization of *Arabidopsis thaliana* solanesyl-diphosphate synthase. *Biochem. J.* **370,** 679–686
28. Hsieh, F. L., Chang, T. H., Ko, T. P., and Wang, A. H. (2011) Structure and mechanism of an *Arabidopsis* medium/long-chain-length prenyl pyrophosphate synthase. *Plant Physiol.* **155,** 1079–1090
29. Pirooznia, M., Nagarajan V., and Deng, Y. (2007) GeneVenn: a web application for comparing gene lists using Venn diagrams. *Bioinformation* **10,** 420–422
30. Dereeper, A., Guignon, V., Blanc, G., Audic, S., Buffet, S., Chevenet, F., Dufayard, J. F., Guindon, S., Lefort, V., Lescot, M., Claverie, J. M., and Gascuel, O. (2008) Phylogeny.fr: robust phylogenetic analysis for the non-specialist. *Nucleic Acids Res.* **36,** W465–W469
31. Jones, M. O., Perez-Fons, L., Robertson, F. P., Bramley, P. M., and Fraser, P. D. (2013) Functional characterization of long-chain prenyl diphosphate synthases from tomato. *Biochem. J.* **449,** 729–740
32. Zbierzak, A. M., Kanwischer, M., Wille, C., Vidi, P. A., Giavalisco, P., Lohmann, A., Briesen, I., Porfirova, S., Bréhélin, C., Kessler, F., and Dörmann, P. (2010) Intersection of the tocopherol and plastoquinol metabolic pathways at the plastoglobules. *Biochem. J.* **425,** 389–399
33. Karamoko, M., Cline, S., Redding, K., Ruiz, N., and Hamel, P. P. (2011) Lumen thiol oxidoreductase 1, a disulfide bond-forming catalyst, is required for the assembly of photosystem II in *Arabidopsis*. *Plant Cell* **23,** 4462–4475
34. Lichtenthaler, H. K., and Miehé, J. A. (1997) Fluorescence imaging as a diagnostic tool for plant stress. *Trends Plant Sci.* **2,** 316–320
35. Müller, P., Li, X. P., and Niyogi, K. K. (2001) Non-photochemical quenching. A response to excess light energy. *Plant Physiol.* **125,** 1558–1566
36. Maeda, H., and DellaPenna, D. (2007) Tocopherol functions in photosynthetic organisms. *Curr. Opin. Plant Biol.* **10,** 260–265
37. Kawamukai, M. (2009) Biosynthesis and bioproduction of coenzyme Q10 by yeasts and other organisms. *Biotechnol. Appl. Biochem.* **53,** 217–226
38. Zybailov, B., Rutschow, H., Friso, G., Rudella, A., Emanuelsson, O., Sun, Q., and van Wijk, K. J. (2008) Sorting signals, N-terminal modifications and abundance of the chloroplast proteome. *PLoS One* **3,** e1994
39. Ferro, M., Brugière, S., Salvi, D., Seigneurin-Berny, D., Court, M., Moyet, L., Ramus, C., Miras, S., Mellal, M., Le Gall, S., Kieffer-Jaquinod, S., Bruley, C., Garin, J., Joyard, J., Masselon, C., and Rolland, N. (2010) AT_CHLORO, a comprehensive chloroplast proteome database with subplastidial localization and curated information on envelope proteins. *Mol. Cell. Proteomics* **9,** 1063–1084
40. Vidi, P. A., Kanwischer, M., Baginsky, S., Austin, J. R., Csucs, G., Dörmann, P., Kessler, F., and Bréhélin, C. (2006) Tocopherol cyclase (VTE1) localization and vitamin E accumulation in chloroplast plastoglobules lipoprotein particles. *J. Biol. Chem.* **281,** 11225–11234
41. Austin, J. R., 2nd, Frost, E., Vidi, P. A., Kessler, F., and Staehelin, L. A. (2006) Plastoglobules are lipoprotein subcompartments of the chloroplast that are permanently coupled to thylakoid membranes and contain biosynthetic enzymes. *Plant Cell* **18,** 1693–1703
42. Lundquist, P. K., Poliakov, A., Giacomelli, L., Friso, G., Appel, M., McQuinn, R. P., Krasnoff, S. B., Rowland, E., Ponnala, L., Sun, Q., and van Wijk, K. J. (2013) Loss of plastoglobule kinases ABC1K1 and ABC1K3 causes conditional degreening, modified prenyl-lipids, and recruitment of the jasmonic acid pathway. *Plant Cell* **25,** 1818–1839
43. Martinis, J., Glauser, G., Valimareanu, S., and Kessler, F. (2013) A chloroplast ABC1-like kinase regulates vitamin E metabolism in *Arabidopsis*. *Plant Physiol.* **162,** 652–662
44. Kirchhoff, H. (2008) Molecular crowding and order in photosynthetic membranes. *Trends Plant Sci.* **13,** 201–207
45. Eugeni Piller, L., Abraham, M., Dörmann, P., Kessler, F., and Besagni, C. (2012) Plastid lipid droplets at the crossroads of prenylquinone metabolism. *J. Exp. Bot.* **63,** 1609–1618
46. Ytterberg, A. J., Peltier, J. B., and van Wijk, K. J. (2006) Protein profiling of plastoglobules in chloroplasts and chromoplasts. A surprising site for differential accumulation of metabolic enzymes. *Plant Physiol.* **140,** 984–997
47. Hundal, T., Forsmark-Andrée, P., Ernster, L., and Andersson, B. (1995) Antioxidant activity of reduced plastoquinone in chloroplast thylakoid membranes. *Arch. Biochem. Biophys.* **324,** 117–122